

## **EFFICIENT MODAL BASIS SELECTION CRITERIA FOR REDUCED-ORDER NONLINEAR SIMULATION**

**Adam Przekop<sup>1</sup> and Stephen A. Rizzi<sup>2</sup>**

<sup>1</sup> National Institute of Aerospace  
Hampton, VA 23666, USA  
E-mail: adam@nianet.org

<sup>2</sup>NASA Langley Research Center  
Hampton, VA 23681, USA  
E-mail: Stephen.A.Rizzi@nasa.gov

**Keywords:** Reduced-order nonlinear simulation, proper orthogonal decomposition, modal assurance criterion, modal expansion theorem.

### **ABSTRACT**

A modal basis selection technique for a reduced-order nonlinear numerical simulation with application to two-dimensional structures is presented as a two-step procedure. A system identification analysis is first performed using proper orthogonal decomposition. Using these results, a set of load-invariant bases consisting of the normal modes is next selected. Two criteria for making the basis selection are offered; one using the modal assurance criterion and the other using the modal expansion theorem. The quality of the subsequent reduced-order analyses are examined through comparison with computationally intensive finite element nonlinear simulations in physical degrees-of-freedom. A clamped flat isotropic plate under a random acoustic loading is considered to demonstrate the procedure. It is found that the subject procedure enables formation of an accurate and computationally efficient reduced-order system applicable to a broad range of loading conditions.

### **1. INTRODUCTION**

Structural dynamic response analysis of complex aerospace components requires application of the finite element (FE) method. Due to extreme loading conditions associated with high-speed flight regimes, e.g. combined aerodynamic, acoustic, thermal, and mechanical loads, a large deflection nonlinear response analysis must often be considered. Furthermore, the uncertainty of the loadings or their random characteristics may require extended simulation times to obtain statistically meaningful results. Of the commercially available tools satisfying this analysis requirement, none do so in a computationally efficient manner. In particular, the cost of a nonlinear FE analysis in physical degrees-of-freedom (DoFs) can easily become prohibitive. Consequently, development of nonlinear reduced-order FE-based analyses is sought.

The quality of any reduced-order analysis depends on the selection of the transformation basis functions. An insufficient modal basis can yield inaccurate response predictions, which may lack essential response characteristics, e.g. autoparametric resonance. While it has been demonstrated that expansion of the modal basis can improve the quality of the reduced-order analysis predictions, excessive basis expansion diminishes its computational advantage. There exists, therefore, a strong incentive to determine a basis which will produce the desired accuracy, yet limit the associated computational expense. Moreover, determination of a modal basis applicable over a broad range of response regimes is also advantageous to avoid repetition of the modal reduction process with each change in loading condition.

In consideration of the above requirements, a procedure for a reliable and efficient modal basis selection is offered as a two-step process. First, a proper orthogonal decomposition (POD) analysis [1-3] is conducted permitting identification of the dominant vibration characteristics of a system in terms of the proper orthogonal values (POVs) and their corresponding proper orthogonal modes (POMs). The POD analysis can be based on a short, but representative, record of the nonlinear dynamic response. Such data may be acquired from a test or, as in the present study, by performing a nonlinear FE simulation in physical DoFs. If a single POD analysis is to be performed, it is imperative that it captures all the nonlinear dynamics of interest. Therefore, analysis of the most severe loading condition under consideration is typically sought. Since the POMs can change as the loading condition changes [4], they do not themselves form the preferred basis as the nonlinear modal basis transformation would potentially need to be repeated for each loading condition. Instead, the second step in the procedure determines a set of load-invariant normal modes which resemble the selected set of POMs. This process can alternatively be performed using the modal assurance criterion (MAC) [5] or the modal expansion theorem [6].

A POD/MAC modal basis selection technique was previously investigated by the authors on simple one-dimensional structures [7] and was found to be a reliable method to guide the selection of modal basis and improve the efficiency of the reduced-order analysis. The objective of the present study is to investigate its applicability to more complex and larger two-dimensional structural members. A clamped aluminum plate under a uniformly distributed random acoustic loading is chosen to demonstrate the approach.

## **2. FORMULATION**

The system identification process by means of a POD analysis is next described and two alternative modal basis selection criteria employing the MAC and the modal expansion theorem are introduced. The previously developed modal system reduction by an indirect nonlinear stiffness evaluation procedure [8, 9] is briefly summarized and the computational cost associated with it is quantified.

### **2.1 System identification – Proper Orthogonal Decomposition**

When physical DoFs are chosen to characterize the response, the snapshot matrix  $\mathbf{X}$  can be formed as an accumulation of  $n$  instantaneous displacement, velocity, or acceleration response fields. In the current analysis, displacement fields, each containing a selected set of  $N$  degrees-of-freedom, are used resulting in a snapshot matrix of size  $n \times N$ . The sample rate and spatial resolution of the snapshot matrix must be sufficient to resolve the system's temporal and spatial characteristics of interest. The correlation matrix  $\mathbf{R}$ , of size  $N \times N$  is formed as

$$\mathbf{R} = \frac{1}{n} \mathbf{X}^T \mathbf{X}. \quad (1)$$

An eigenanalysis of the correlation matrix is next performed, i.e.,

$$[\mathbf{R} - \lambda \mathbf{I}] \mathbf{p} = \mathbf{0} \quad (2)$$

to obtain a POM matrix  $\mathbf{P} = [\mathbf{p}_1 \ \mathbf{p}_2 \ \dots \ \mathbf{p}_{n\text{DOF}}]$  and the diagonal POV matrix,  $\lambda$ , both of size  $N \times N$ . Each POV is a measure of the corresponding POM activity, i.e., the higher the POV, the greater the contribution of a corresponding POM to the dynamic response.

POMs obtained for an undamped linear system are identical to the normal modes [1, 2]. For the problem of interest, i.e. flat or shallowly curved isotropic panels, the normal modes can be characterized as being either transverse-dominated or in-plane dominated. Low frequency, transverse-dominated modes are those modes for which the maximum amplitude of the transverse displacement component is much larger than the maximum amplitude of the in-plane displacement component. High frequency, in-plane dominated modes are those modes for which the maximum amplitude of the in-plane displacement component is much larger than the maximum amplitude of the transverse displacement component. The POM matrix, however, is fully populated, creating an inherent mismatch between the POMs and the normal modes of the system under analysis. This inconsistency can make the identification of normal modes similar to POMs difficult. To mitigate this problem, the POD procedure is performed independently for each DoF type of interest by partitioning the snapshot matrix. In the subsequent POD analyses, five out of six available DoF types, i.e., transverse displacement  $w$ , two in-plane displacements  $u$  and  $v$ , and two out-of-plane rotations  $\phi_x$  and  $\phi_y$ , are analyzed. The sixth DoF type, the rotation about the normal to the plate surface  $\phi_z$ , also called the drilling DoF, is not considered. Because the drilling DoF is not included in all shell element formulations, it was not used in the present study to allow the procedure to be applicable to any shell element formulation. By adopting this approach, the size of each individual DoF snapshot matrix  $\mathbf{X}$  is reduced to  $n \times m$ , where  $m$  is the number of nodes, and the size of each individual correlation matrix  $\mathbf{R}$ , POM matrix  $\mathbf{P}$ , and POV matrix  $\lambda$  is reduced to  $m \times m$ .

## 2.2 Modal basis selection

The contribution of each POM to the overall dynamic response is given by

$$\chi_i = \frac{\lambda_i}{\sum_{j=1}^m \lambda_j} \quad i = 1, \dots, m \quad (3)$$

where  $\chi_i$  is the  $i$ -th POM participation factor. The sum of all POM participation factors is unity. When the most contributing  $M$  POMs are selected, their cumulative participation,  $\nu$ , can be expressed as

$$\nu = \sum_{i=1}^M \chi_i \quad 0 < \nu \leq 1 \quad (4)$$

Retention of only the selected  $M$  POMs reduces the size of  $\mathbf{P}$  to  $m \times M$ .

As previously indicated, the direct use of POMs for the basis is not preferred as they may be load specific. Instead a set of normal modes which resemble the POMs is sought using one of the approaches next discussed.

#### *Modal Assurance Criterion*

An engineering measure of the similarity of two vectors is the MAC value [5]. By computing the MAC values for each pair of the selected POMs  $\mathbf{p}$  and all the normal modes  $\boldsymbol{\varphi}$ , i.e.,

$$MAC(\mathbf{p}_k, \boldsymbol{\varphi}_l) = \frac{|\mathbf{p}_k^T \boldsymbol{\varphi}_l|^2}{(\mathbf{p}_k^T \mathbf{p}_k)(\boldsymbol{\varphi}_l^T \boldsymbol{\varphi}_l)} \quad \begin{matrix} k = 1, \dots, M \\ l = 1, \dots, N \end{matrix} \quad (5)$$

the MAC matrix can be formed.

Note that since each DoF is individually considered, separate MAC matrices for each DoF type are formed. While the total number of normal mode vectors,  $N$ , is unaffected by partitioning, their lengths are reduced from  $N$  to  $m$ . The MAC matrices therefore have the size of  $N \times M$  for the five DoF types considered.

Once the MAC matrices are determined, a MAC threshold level is used to identify the normal modes best resembling the selected POMs. A threshold of  $MAC \geq 0.5$  was used in this work. A higher threshold value would identify fewer modes, generally leading to a less accurate but more computationally efficient solution. A lower threshold value would identify a greater number of modes, leading to a more accurate but less computationally efficient solution.

The MAC-based normal modes selection approach, while straightforward to implement, may not always be sufficient. In a strongly nonlinear response regime, it is not guaranteed that the POD analysis will yield POMs bearing much resemblance to the normal modes. Consequently, multiple normal modes may be required to represent a single POM. This objective may be achieved by lowering the MAC threshold value, however, doing so may not be intuitive and the desired threshold may vary between different POMs. Therefore, a more systematic approach is considered.

#### *Modal Expansion Theorem*

A single POM may be decomposed into a linear combination of normal modes according to the expansion theorem [6]

$$\mathbf{p}_i = \sum_{j=1}^L c_{ij} \boldsymbol{\varphi}_j \quad (6)$$

where  $c_{ij}$  are the expansion coefficients. Since the normal modes  $\boldsymbol{\varphi}$  are orthogonal, i.e.,

$$\boldsymbol{\varphi}_k^T \boldsymbol{\varphi}_l = 0 \quad k \neq l \quad (7)$$

pre-multiplying Eq. (6) by  $\boldsymbol{\varphi}_k^T$  yields

$$s_{ik} = c_{ik} \boldsymbol{\varphi}_k^T \boldsymbol{\varphi}_k = \boldsymbol{\varphi}_k^T \mathbf{p}_i. \quad (8)$$

The coefficient matrix  $\mathbf{S}$  may be formed by evaluating Eq. (8) over all selected POMs,

( $i = 1, \dots, M$ ) and over all normal modes ( $k = 1, \dots, N$ ), and may be written the compact form

$$\mathbf{S} = \mathbf{\Phi}^T \mathbf{P} . \quad (9)$$

Similar to MAC matrices, one  $\mathbf{S}$  matrix is formed for every DoF type and the size of each  $\mathbf{S}$  matrix is  $N \times M$ .

Each column of  $\mathbf{S}$  corresponds to a specific POM. Because the POMs  $\mathbf{P}$  used to compute the  $\mathbf{S}$  matrix are not normalized, it is convenient to normalize each column of this matrix to unity so that a single threshold value can be used to identify the most significant normal modes. In this work, those modes above a threshold value of 0.5 were included in the basis.

When Eq. (8) is squared and substituted into Eq. (5), the relationship between the MAC and expansion theorem approaches is established as

$$MAC(\mathbf{p}_k, \boldsymbol{\phi}_l) = \frac{s_{kl}^2}{(\mathbf{p}_k^T \mathbf{p}_k)(\boldsymbol{\phi}_l^T \boldsymbol{\phi}_l)} \quad \begin{matrix} k = 1, \dots, M \\ l = 1, \dots, N \end{matrix} \quad (10)$$

Despite the fact that the two approaches are similar in terms of the underlying theory, their functionality is not alike. The MAC-based approach considers only the absolute measure of the similarity between a POM and a normal mode, as quantified by a MAC value. The expansion theorem approach identifies a truncated set of the normal modes which linearly superpose to obtain the POM shape. Consequently, the expansion theorem approach will always identify at least one normal mode for each POM irrespective of the threshold value, where the MAC-based approach may fail to identify any modes if the threshold value is too high. Therefore, the number of selected POMs,  $M$ , and the number of identified normal modes generally differ.

### 2.3 Nonlinear reduced-order analysis

Once a set of basis functions is selected using one of the above approaches, the nonlinear modal reduction of the system can proceed. A reduced-order method gains its computational advantage by reducing the size of the system in physical DoFs (full order) to a much smaller system expressed in generalized coordinates (reduced-order). For the problem of interest, the equation of motion in physical DoFs can be expressed as

$$\mathbf{M}\ddot{\mathbf{x}}(t) + \mathbf{C}\dot{\mathbf{x}}(t) + \mathbf{f}_{NL}(\mathbf{x}(t)) = \mathbf{f}(t), \quad (11)$$

where  $\mathbf{M}$  and  $\mathbf{C}$  are the structural mass and damping matrices, and  $\mathbf{x}$ ,  $\mathbf{f}_{NL}$ , and  $\mathbf{f}$  are the physical displacement, nonlinear restoring force, and excitation force vectors, respectively. By applying the modal transformation

$$\mathbf{x}(t) = \mathbf{\Phi} \mathbf{q}(t), \quad (12)$$

the reduced-order equation of motion becomes

$$\tilde{\mathbf{M}}\ddot{\mathbf{q}}(t) + \tilde{\mathbf{C}}\dot{\mathbf{q}}(t) + \tilde{\mathbf{f}}_{NL}(q_1(t), q_2(t), \dots, q_L(t)) = \tilde{\mathbf{f}}(t) \quad (13)$$

where  $\mathbf{q}$  is a generalized coordinate vector and  $\mathbf{\Phi}$  is a matrix containing  $L$  selected normal modes. The modal nonlinear restoring force in Eq. (13) can be expressed as

$$\tilde{\mathbf{f}}_{\text{NL}} = \mathbf{\Phi}^T \mathbf{f}_{\text{NL}} . \quad (14)$$

When mass-normalized normal modes are used as the basis functions, the modal mass and damping matrices can be expressed as  $\tilde{\mathbf{M}} = \mathbf{\Phi}^T \mathbf{M} \mathbf{\Phi} = [\mathbf{I}]$  and  $\tilde{\mathbf{C}} = \mathbf{\Phi}^T \mathbf{C} \mathbf{\Phi} = [2\zeta_r \omega_r]$ , where  $\omega_r$  and  $\zeta_r$  are the undamped natural frequencies and the viscous damping factors, respectively. The modal excitation force vector is  $\tilde{\mathbf{f}} = \mathbf{\Phi}^T \mathbf{f}$ .

The system reduction utilized in this study is based on the indirect approach employing a nonlinear stiffness evaluation procedure [8, 9]. The procedure expresses the  $r$ -th component of the nonlinear modal restoring force vector as

$$\tilde{f}_{\text{NL}}^r(q_1, \dots, q_L) = \sum_{j=1}^L d_j^r q_j + \sum_{j=1}^L \sum_{k=j}^L a_{jk}^r q_j q_k + \sum_{j=1}^L \sum_{k=j}^L \sum_{l=k}^L b_{jkl}^r q_j q_k q_l \quad r = 1, \dots, L, \quad (15)$$

where  $d$ ,  $a$ , and  $b$  are the linear, quadratic, and cubic modal stiffness coefficients, and  $L$  is the number of selected modes. Different combinations of scaled normal modes form a set of prescribed displacement fields. The normal mode vectors are scaled by the generalized coordinates  $q$  to obtain physically meaningful magnitudes. Using a nonlinear static FE analysis, the nonlinear restoring forces corresponding to each prescribed displacement field are computed in physical DoFs and transformed to the generalized coordinates per Eq. (14). As the vector  $\tilde{\mathbf{f}}_{\text{NL}}$  and the generalized coordinates  $q$  are known, Eq. (15) constitutes a system of algebraic equations from which the linear, quadratic and cubic modal stiffness coefficients may be determined. The number of unknown coefficients, and hence the number of nonlinear static solutions required for a transformation utilizing  $L$  modes is

$$\text{Number of NL Static Solutions} = 3 \binom{L}{1} + 3 \binom{L}{2} + \binom{L}{3} \quad L \geq 3 \quad (16)$$

where

$$\binom{L}{k} = \frac{L!}{k!(L-k)!} . \quad (17)$$

Note that the three terms in Eq. (16) reflect the number of linear, quadratic, and cubic modal stiffness coefficients, respectively. The number of nonlinear static solutions can be viewed as a measure of the fixed cost of the reduced-order analysis, as the modal reduction must be performed regardless of the simulated response time to be eventually computed.

### 3. RESULTS

The flat plate under investigation measured  $355.6 \times 254.0 \times 1.016$  mm and had fully clamped boundary conditions on all four edges. Isotropic material properties for aluminum were used: Young modulus  $E = 73.11$  GPa, shear modulus  $G = 27.59$  GPa, and mass density  $\rho = 2763$  kg/m<sup>3</sup>.

The ABAQUS FE model used for both the physical DoF analysis and the normal modes analysis consisted of 8960 ABAQUS S4R shell elements, each measuring  $3.175 \times 3.175$  mm. The S4R is a quadrilateral element with a large strain formulation and incorporates first order

shear deformation theory. Each element has four nodes, each with 6 DoFs, resulting in a system size of approximately 55,000 DoFs. The origin of the global coordinate system was collocated with the lower left corner of the plate so that the  $x$ -axis was aligned with the longer plane edge, and the  $y$ -axis was aligned with the shorter plane edge. A fixed modal damping value of  $14.66 \text{ s}^{-1}$  was applied in the dynamic response analysis giving a 1.07% critical damping for the fundamental mode at 109.34 Hz.

### 3.1 Nonlinear system identification and modal reduction

The nonlinear response analysis of the plate in physical DoFs was performed via explicit integration using the ABAQUS/Explicit FE code. An automatically determined integration time step, referenced in ABAQUS documentation as ‘element-by-element,’ was used. This approach is known to yield a conservative integration time step [10].

The plate was subjected to a uniformly distributed normal acoustic loading. Band-limited random acoustic loading with a flat frequency distribution was generated by summing equal amplitude sine waves, each with random phase, at a frequency resolution of 0.61 Hz in the frequency range 0 – 1024 Hz. An overall sound pressure level (OASPL) of 154 dB (re: 20  $\mu\text{Pa}$ ) was applied. The total simulation time for the POD analysis was 1.0 s. The initial 0.5 s containing the transient response was removed, leaving 0.5 s of fully developed response for the POD analysis. A total of  $n = 10,000$  displacement field snapshots at an output sampling rate of 50  $\mu\text{s}$  were captured at every forth node in both  $x$  and  $y$  coordinate directions. The spatial resolution of the output data for each of the five DoF types was therefore 12.7 mm, and the number of output nodes was  $m = 609$ . The selected simulation time and the chosen resolution of the temporal and spatial outputs provided sufficient data for the POD analysis while keeping the required output volume reasonable. Each of the five snapshot matrices were of size of  $10,000 \times 609$ , resulting in five correlation matrices each of size of  $609 \times 609$ .

The normal mode analysis of the plate was performed using the ABAQUS/Standard FE code. The subspace solver was used to compute all mass-normalized normal modes present within a 50 kHz bandwidth. Five displacement components were output at each node. To be consistent with the POD analysis, only every fourth node was utilized in the modal basis identification process. However, all DoFs were used in the solution of the modal stiffness coefficient for the subsequent reduced-order analysis. A list of modes relevant to the basis selection is presented in the shaded cells of Table 1.

### 3.2 Selected modal bases

#### *MAC- and expansion theorem-based approaches*

The POVs and corresponding POMs were computed individually for the five DoF types per Eq. (2). This enabled subsequent computation of the POV participations per Eq. (3) by which each group of POMs was arranged in a descending order. For each DoF type, the 16 POMs with the largest POV participations were considered. For the selected set of POMs, the cumulative POV participation factors were computed per Eq. (4). These factors for the transverse displacement  $w$ ,  $x$ - and  $y$ -direction in-plane displacements  $u$  and  $v$ , and the rotations about the  $x$  and  $y$  axes  $\phi_x$  and  $\phi_y$ , were found to be 99.98, 99.74, 99.78, 99.84, and 99.63%, respectively. Next, the MAC-based and the expansion theorem-based mode selection criteria were considered. The normal modes with MAC values of 0.5 or greater were identified per Eq. (5) and the expansion coefficients  $S$  of value 0.5 or greater (after normalization) were identified per Eq. (9).

Table 1: Selected eigenanalysis and basis selection results

Transverse Modes		T Bases		T+I Bases		In-plane Modes		T+I Bases	
Mode Number	Frequency (Hz)	6 (6T)	16 (16T)	MAC (16T + 7I)	Exp. (16T + 19I)	Mode Number	Frequency (Hz)	MAC (16T + 7I)	Exp. (16T + 19I)
1	109.3	+	+	+	+	391	15,603	+	+
4	290.2	+	+	+	+	520	20,448	+	+
8	494.1	+	+	+	+	558	21,917	+	+
11	641.7	+	+	+	+	634	24,902	+	+
12	657.7	+	+	+	+	708	27,912	+	+
19	991.1	+	+	+	+	785	30,812	+	+
22	1156.0		+	+	+	834	32,736		+
23	1194.0		+	+	+	862	33,667		+
28	1352.9		+	+	+	895	34,639		+
30	1493.5		+	+	+	991	38,971		+
35	1675.5		+	+	+	1012	39,515		+
40	1833.3		+	+	+	1098	42,830		+
46	2162.0		+	+	+	1099	42,945	+	+
47	2165.9		+	+	+	1136	44,300		+
48	2212.5		+	+	+	1173	45,876		+
59	2675.8		+	+	+	1179	46,078		+
						1206	47,085		+
						1234	48,405		+
						1257	49,158		+

Both the MAC and the expansion theorem selection approaches identified the same set of 16 transverse (T) displacement normal modes, as shown in columns 5 and 6 of Table 1. The same set of normal modes was obtained when considering either the  $w$ ,  $\phi_x$  or  $\phi_y$  DoFs. The results of the selection process differed, however, between the two approaches when the  $u$  and  $v$  in-plane displacements were considered. Recall that the objective was to identify a set of normal modes resembling the most contributing 16  $u$  and 16  $v$  POMs. The MAC-based approach, however, was able to identify an in-plane modal basis corresponding to only the first three  $u$  and first five  $v$  POMs. This basis consisted of seven in-plane modes, see column 9 of Table 1. For  $u$  in-plane POMs, there were no normal modes exceeding the MAC threshold for POM number 4 and higher. For the  $v$  in-plane POMs, normal modes exceeding the MAC threshold were identified for POMs 1-5, 7 and 12. However, since POM number 6 has a greater participation than POM number 7, and since POM numbers 8-11 have greater participation than POM number 12, the basis was selected by restricting the set identified to the highest consecutive ranking, i.e. POM numbers 1-5. Representing only the first three  $u$  and the first five  $v$  POMs reduced the cumulative POV participation from 99.74 to 89.61% and from 99.78 to 97.01% for the  $u$  and  $v$  DoF types, respectively. The expansion theorem-based approach resulted in the identification of the  $u$  and  $v$  in-plane displacement basis consisting of 19 in-plane (I) modes, i.e., see column 10 of Table 1. The expansion theorem approach, by design, represented all of the selected  $u$  and  $v$  in-plane POMs with at least one normal mode. Consequently, the MAC-derived basis consisted of 23 normal modes (16 T + 7 I), and the expansion theorem-derived basis consisted of 35 normal modes (16 T + 19 I). As intended and expected, for the parameters considered in both approaches, the expansion theorem-based selection method resulted in identification of a larger set of normal modes. Note that the 7 in-plane modes identified by MAC-based approach are the subset of the 19 in-plane modes identified by the expansion theorem-based approach.

To illustrate how the results of the MAC-based and the expansion theorem-based approaches differ, the most contributing  $v$  in-plane POM is presented in Figure 1(a). The MAC-based approach identified normal modes 391, Figure 1(b), and 520, Figure 1(c), to represent this POM. The expansion theorem-based approach additionally identified mode 558, Figure 1(d), which has the MAC value lower than 0.5.

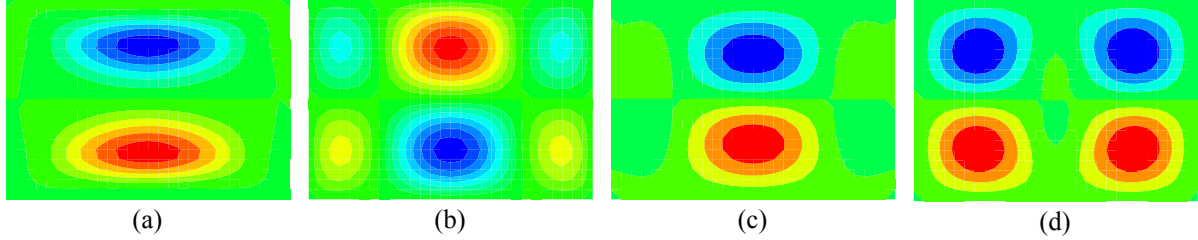


Figure 1.  $v$  in-plane displacement: (a) POM number 1; (b) mode 391, MAC=0.61, exp. coeff.  $s=-0.91$ ; (c) mode 520, MAC=0.84,  $s=1.00$ ; (d) mode 558, MAC=0.33,  $s=0.78$ .

Finally, it is worthwhile to note that all the transverse displacement POMs and the identified transverse displacement normal modes had symmetric displacement distributions. All the in-plane displacement POMs and the identified in-plane displacement normal modes had anti-symmetric distributions simultaneously in both  $x$ - and  $y$ -directions.

#### *Traditional approaches*

The traditional approach of selecting a modal basis by neglecting the high-frequency in-plane behavior was undertaken for comparative purposes. Considering the structural symmetry and the excitation bandwidth, the lowest symmetric transverse displacement modes with natural frequencies up to 1024 Hz were selected. This resulted in the basis shown in column 3 of Table 1. Any difference between results obtained using the traditional 6-mode T basis and either of the T+I mode bases may be attributed to two factors: 1) the lack of high-frequency in-plane modes in the basis, and 2) the lack of low-frequency transverse modes beyond the excitation bandwidth. To help discriminate these effects, an additional basis consisting of all 16 transverse displacement modes included in the MAC- and the expansion theorem-selected bases was considered, see column 4 in Table 1.

#### *Computational cost of modal reduction*

When assessing the quality of results subsequently presented, it is important to bear in mind the computational effort required. While any of the presented reduced-order solutions obtained with 6, 16, 23, or 35 generalized coordinates require significantly less computational effort than the analysis in physical coordinates, the differences between them vary markedly. The required number of nonlinear static solutions for the above bases is 83, 968, 2599, and 8435, respectively. Therefore, the reduced-order solution with the highest fidelity (35 mode basis) is over 100 times more expensive than the one with the lowest fidelity (6 mode basis).

### **3.3 Nonlinear modal simulation**

The ABAQUS-based implementation of the computer code RANSTEP [7, 9] was used to assess the quality of the reduced-order analyses performed using the various bases identified in Table 1. The assessment was carried out by comparing the displacement and stress response power spectral densities (PSDs) obtained from the reduced-order analyses with those obtained from the physical DoFs analyses. The simulation in physical DoFs was conducted as

previously described, but with the total simulation time extended to 2.1384 s. After removing the initial 0.5 s transient, the fully developed response of 1.6384 s duration was used to compute the PSDs, each with a frequency resolution of 0.61 Hz. The reduced-order nonlinear system was integrated using a 4<sup>th</sup> order Runge-Kutta scheme with a fixed time step of 1  $\mu$ s. For the reduced-order analyses, the simulation duration, output sampling, and post-processing were the same as those used in the physical DoF analyses.

### *Displacement results*

All displacement results presented herein were obtained at the quarter-quarter span location, i.e., at the (88.9, 63.5) mm coordinate node. The choice of this location was made because of a desire to scrutinize both transverse and in-plane displacement components. Since the 23- and 35-mode bases included only anti-symmetric in-plane modes, interrogation of the center point response would always produce a zero-valued in-plane displacement response.

The displacement results obtained at a low excitation level of 106 dB OASPL are presented in Figure 2 and Figure 3 for the transverse displacement  $w$  and in Figure 4 for the in-plane displacement  $u$ . All transverse displacement results are in a very good agreement with those obtained in physical DoFs. While the reduced-order solutions with 16, 23, and 35 modes appear identical, there exists a very minor difference in the 6-mode basis results above 700 Hz. The difference, despite being inconsequential to the overall response, points to the importance of including the low-frequency transverse modes present beyond the excitation bandwidth. The in-plane displacement solution offers a different perspective. Due to the lack of in-plane displacement representation, the 6- and 16-mode bases are unable to produce any displacement response. As seen in Figure 4, the 35-mode basis matches the physical DoFs solution better than does the 23-mode basis. This result is expected since the 35-mode basis contains 19 in-plane modes, and the 23-mode basis contains only 7 in-plane modes. A more significant observation, however, is that the in-plane displacement results require more normal modes than the transverse displacement results to obtain comparable performance relative to the physical DoFs solution. This fact is indicated, for example, by the difference seen between the physical DoFs solution and the 35-mode basis solution in the neighborhood of 200 Hz. It is also important to note that the nonlinear modal reductions performed using the T+I bases are applicable in this nearly linear response regime, even though the POD analysis used in their selection was performed at a highly nonlinear level of 154 dB.

When the  $u$  in-plane displacement PSD is examined at the 154 dB excitation level, the in-plane response obtained with the 35-mode basis also compares better with the physical DoFs solution than the 23-mode basis, as shown in Figure 5. The overall comparison of results obtained with these two bases relative to the physical DoFs solution is, however, less favorable when compared with the 106 dB excitation level results. The quality of the transverse displacement  $w$  PSD results at this level can be clearly classified into two groups. The 6- and 16-mode T bases without the in-plane displacement representation, shown in Figure 6, perform visibly worse when compared to the 23- and 35-mode T+I bases with the in-plane displacement representation, shown in Figure 7. In particular, the transverse displacement solutions obtained with the 6- and 16-mode T bases show excessive peak broadening and shifting towards the higher frequencies. Differences between the 6- and 16-mode T bases, and differences between the 23- and 35-mode T+I bases, however, are relatively insignificant. Therefore, contrary to the 106 dB excitation level case, accurate modeling of the in-plane displacement response strongly influences the quality of the transverse displacement response in the nonlinear response regime.

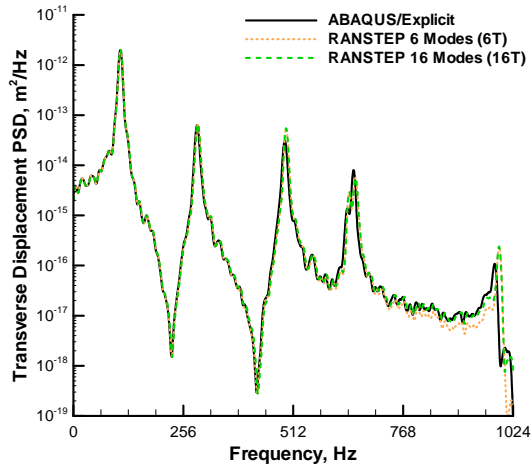


Figure 2. Transverse displacement  $w$  PSD at 106 dB (6- and 16-mode T bases).

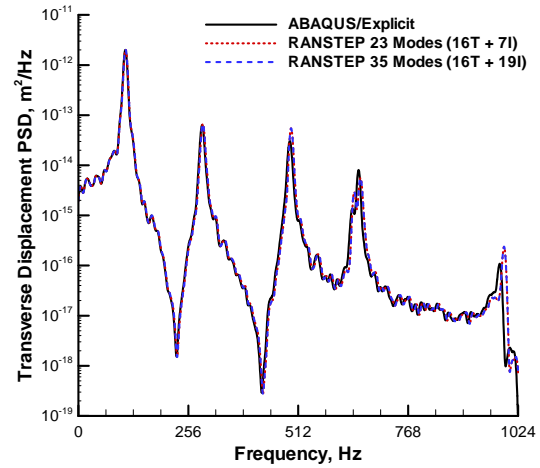


Figure 3. Transverse displacement  $w$  PSD at 106 dB (23- and 35-mode T+I bases).

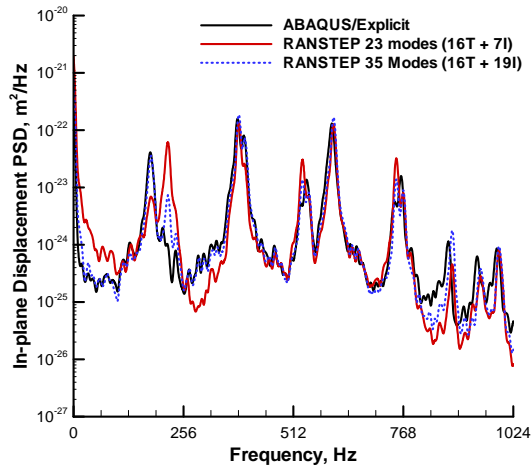


Figure 4. In-plane displacement  $u$  PSD at 106 dB (23- and 35-mode T+I bases).

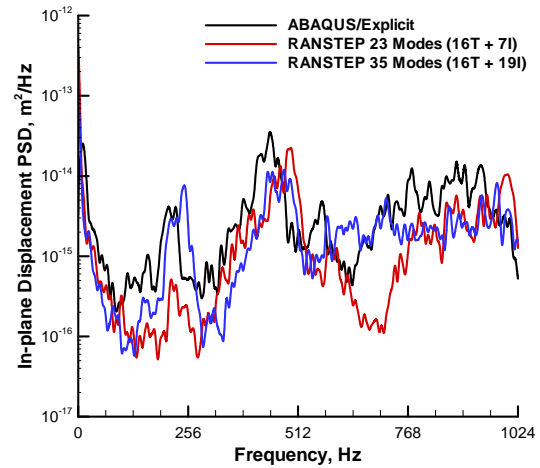


Figure 5. In-plane displacement  $u$  PSD at 154 dB (23- and 35-mode T+I bases).

### Stress results

The normal stress  $\sigma_{yy}$  at the boundary of the longer edge mid-span was next investigated. Because the S4R element has only one integration point at its center, the stress response was recovered at the element center nearest to this point, located at (176.213, 1.588) mm.

Figure 8 and Figure 9 show the stress PSD results at the 106 dB excitation level obtained with 6- and 16-mode T bases, and with the 23- and 35-mode T+I bases, respectively. Since the transverse displacement response component almost exclusively dictates the stress response in this nearly linear response regime, the comparison with the physical DoFs solution is very good for all bases considered. While all four solutions do not perfectly capture the anti-resonant behavior in the bandwidth approximately from 650 to 950 Hz, the differences are insignificant relative to the overall stress response. The most pronounced difference in this frequency bandwidth, however, is noticed in the 6-mode T basis, which again is attributable to the lack of low-frequency transverse modes beyond the excitation bandwidth.

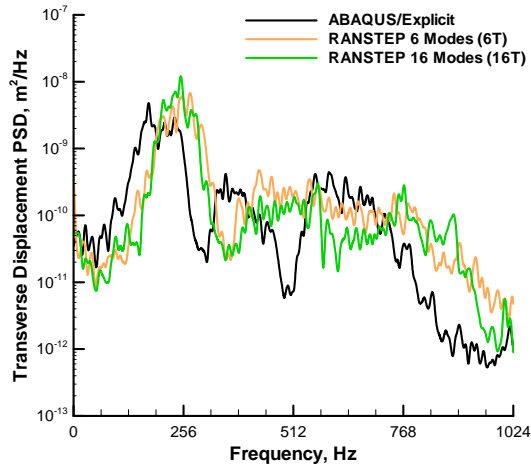


Figure 6. Transverse displacement  $w$  PSD at 154 dB (6- and 16-mode T bases).

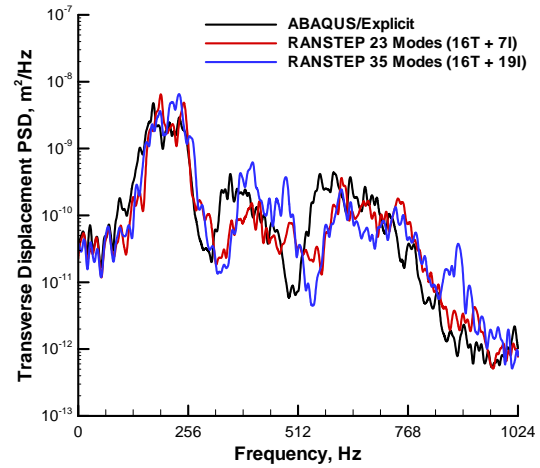


Figure 7. Transverse displacement  $w$  PSD at 154 dB (23- and 35-mode T+I bases).

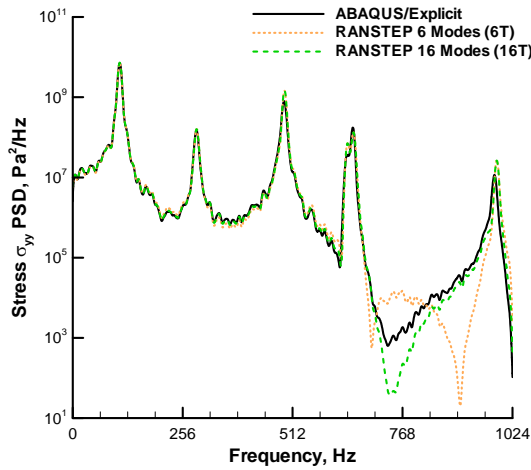


Figure 8. Normal stress  $\sigma_{yy}$  PSD at 106 dB (6- and 16-mode T bases).

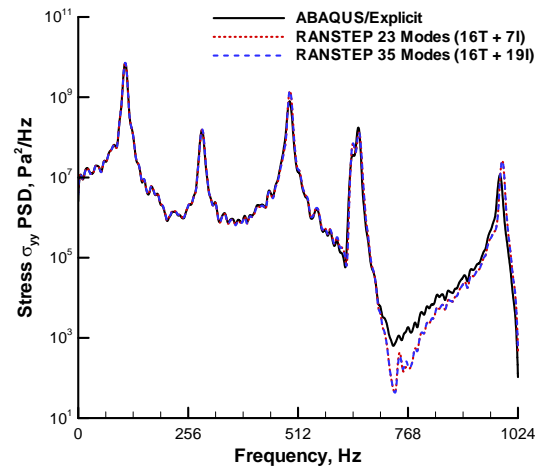


Figure 9. Normal stress  $\sigma_{yy}$  PSD at 106 dB (23- and 35-mode T+I bases).

As the excitation level is increased to 136 dB, the response becomes moderately nonlinear, as presented in Figure 10 and Figure 11. At this response level, it is apparent that inclusion of the in-plane displacement normal modes in the basis has a beneficial effect on the quality of the computed stress response. The results obtained with the 6- and the 16-mode T basis show only small differences between themselves, but show excessive broadening of the peaks relative to the physical DoF solution above approximately 500 Hz. This behavior is not found in the stress response computed with the 23- or the 35-mode T+I basis. While the differences between the 23- and the 35-mode T+I basis become locally distinguishable at this response level, they can be considered to be very minor.

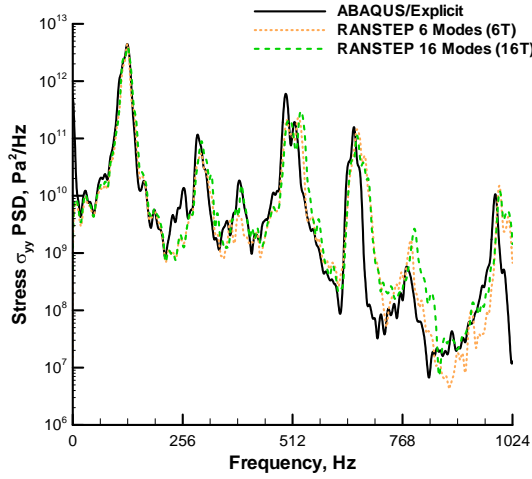


Figure 10. Normal stress  $\sigma_{yy}$  PSD at 136 dB (6- and 16-mode T bases).

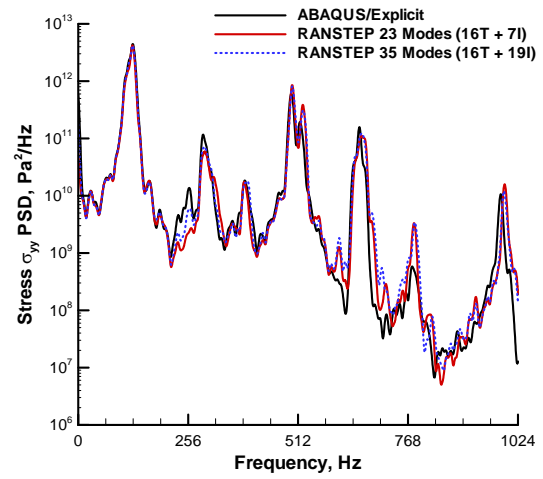


Figure 11. Normal stress  $\sigma_{yy}$  PSD at 136 dB (23- and 35-mode T+I bases).

Results for the strongly nonlinear response at the 154 dB excitation level, originally used to perform the POD, are presented in Figure 12 and Figure 13. Differences noted in the response at 136 dB are further exaggerated at this level. Both the 6- and 16-mode T basis solutions show excessive peak broadening and shifting of the first peak to higher frequencies. Subsequent peaks are indistinguishable. Again, differences between the 6- and the 16-mode T basis solutions are not significant. The quality of the solutions obtained with the 23- and the 35-mode T+I bases are substantially better. In particular, the magnitude of the first peak is captured more accurately and shows almost no excessive shifting or broadening. While excessive shifting and broadening of the second and the third peak is present, these two peaks are readily identifiable and can easily be related to the features of the physical DoFs response. The relative quality of the 23- and the 35-mode T+I basis solutions are comparable, with the 35-mode solution being slightly more accurate in the mid-frequency range.

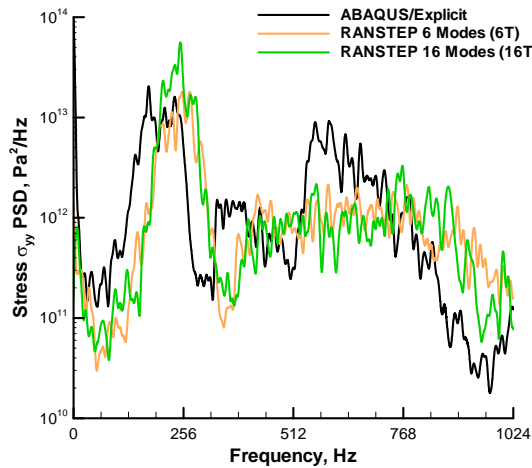


Figure 12. Normal stress  $\sigma_{yy}$  PSD at 154 dB (6- and 16-mode T bases).

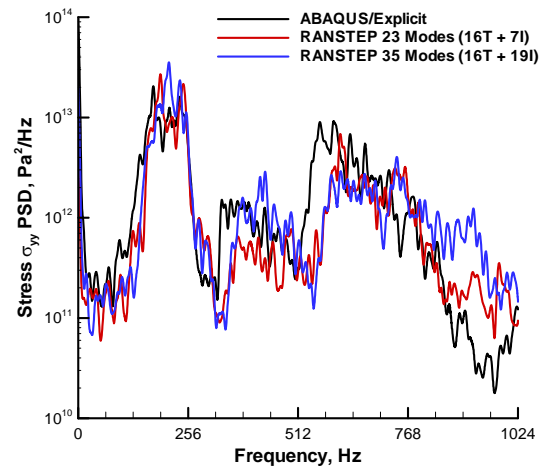


Figure 13. Normal stress  $\sigma_{yy}$  at 154 dB (23- and 35-mode T+I bases).

#### 4. CONCLUDING REMARKS

Two criteria for selecting modal bases for use in a finite element nonlinear reduced-order analysis were presented. Both enable formation of an accurate and computationally efficient reduced-order system applicable to a broad range of loading conditions. Each relies on a system identification step using a POD analysis of the displacement response obtained by a finite element nonlinear simulation in physical DoFs. The previously implemented criterion for correlating the POMs with the normal modes using the MAC was complemented by an alternative criterion employing the modal expansion theorem. Application of both criteria to a two-dimensional structure demonstrated their suitability to structures with a greater modal density than previously considered. For the case studied and analysis parameters selected, the expansion theorem approach resulted in a slight quality improvement over the MAC approach, relative to the finite element nonlinear simulation in physical DoFs. This improvement came, however, at a significant increase in the computational expense. The two methods merit further investigation on a broader sample of structures with a broader set of selection parameters. In general, formation of the modal basis for a nonlinear response analysis was determined to be more challenging with regard to the in-plane displacement modeling than it was for the transverse displacement modeling.

#### REFERENCES

- [1] B. F. Feeny, On proper orthogonal co-ordinates as indicators of modal activity, *Journal of Sound and Vibration*, 255(5), 805-817, 2002.
- [2] B. F. Feeny, R. Kappagantu, On the physical interpretation of proper orthogonal modes in vibrations, *Journal of Sound and Vibration*, 211(4), 607-616, 1998.
- [3] G. Kerschen, J.-C. Golinval, A. F. Vakakis, L. A. Bergman, The method of proper orthogonal decomposition for dynamical characterization and order reduction of mechanical systems: an overview, *Nonlinear Dynamics*, 41(1-3), 147-169, 2005.
- [4] N. Kumar, T. D. Burton, Use of random excitation to develop POD based reduced order models for nonlinear structural dynamics, *Proceedings of the ASME 2007 International Design Engineering Technical Conference and Information in Engineering Conference IDETC/CIE 2007*, DETC2007-35539, Las Vegas, NV, 2007.
- [5] R. J. Allemang, D. L. Brown, A correlation coefficient for modal vector analysis, *Proceedings of The 1st International Modal Analysis Conference*, pp. 110-116, Orlando, FL, 1982.
- [6] J. F. Doyle, *Static and Dynamic Analysis of Structures with An Emphasis on Mechanics and Computer Matrix Methods*. Dordrecht, The Netherlands, Kluwer Academic Publishers, 1991.
- [7] S. A. Rizzi, A. Przekop, System identification guided basis selection for reduced order nonlinear response analysis, *Journal of Sound and Vibration*, in press, doi: 10.1016/j.jsv.2007.12.031.
- [8] A. A. Muravyov, S. A. Rizzi, Determination of nonlinear stiffness with application to random vibration of geometrically nonlinear structures, *Computers and Structures*, 81(15), 1513-1523, 2003.
- [9] S. A. Rizzi, A. Przekop, Estimation of sonic fatigue by reduced-order finite element based analysis, *Structural Dynamics: Recent Advances, Proceedings of the 9th International Conference*, The Institute of Sound and Vibration Research, University of Southampton, Southampton, UK, 2006.
- [10] ABAQUS version 6.6 On-line Documentation, ABAQUS Analysis User's Manual, Section 6.3.3, Abaqus, Inc., 2005.